including stress response and sympathetic activation, being generally observed during exercise around LT. Thus, the aim of this study is to clarify whether running stress activates NA neurons; and if so, if it can be hypothesized that this activation will occur only during exercise above the LT. To address this, we investigated whether running stress activates NA neurons in the A1/A2 by examining the expression of Fos protein, an immediate early gene product, in NA neurons in the A1/A2.

Male Wistar rats (250–300 g) were housed four per cage and kept on a 12-h light:12-h dark cycle with standard laboratory feed and water *ad libitum*. Body weight was measured daily. All the procedures used were in accordance with the NIH Guidelines for Ethical Care of Experimental Animals and were approved by the University of Tsukuba's Experimental Animal Use Committee.

The protocols for the training and the exercise tests were the same as in our previous study [20]. Briefly, rats were initially trained to run 5 days/week for 2 weeks with a graded increase in the speed and duration for 30 m/min/day on a treadmill (KN-73 Natsume, Tokyo, Japan), before they were subjected to an exercise test. This test consisted of running at 15 m/min or 25 m/min a 0° incline for 30 min. The control rats were put on the treadmill without running for 30 min. All exercise tests were performed between 8:00 and 11:30 a.m. to eliminate the effect of basal glucocorticoid level, which is known to increase during the dark phase. After completion of the test, the animals were withdrawn blood from previously inserted jugular catherter for measurements of blood lactate and plasma ACTH concentrations. Blood lactate was measured using an automated glucose-lactate analyzer (2300 Stat Plus, YSI, OH, USA). Plasma samples were obtained by centrifugation and stored at −30 °C until measurement. Plasma concentrations of ACTH were measured using commercially available kits (ICN Biomedicals, Costa Mesa, CA) with a detection limit of <4 pg/ml. The coefficient of intra-assay variation was 7.2%. For immunohistochemistry, the animals were returned to their home cage. A hundred twenty minutes after the initiation of the test, they were anesthetized with sodium pentobarbital (50 mg/kg, i.p.) and perfused first with saline and then with 5% acrolein in 0.1 M phosphate buffer (PB, pH 7.4). The brains were quickly removed and immersed for more than 24 h in PB containing 30% sucrose. Frozen serial frontal sections (40 μm thick) of the brain were made using a cryomicrotome. The sections were then processed for immunohistochemistry.

A sensitive immunohistochemical method of that employs a free-floating technique was used as previously described [20]. Briefly, the cryosections were washed with PB and immersed sequentially in the following solutions: (1) 0.5% sodium metaperiodate in PB for 20 min, (2) 1% sodium borohydride in PB for 20 min, (3) 1% normal goat serum and 0.2% Triton X-100 in PB (GPB) for 1 h, (4) a rabbit polyclonal antibody against Fos protein (Oncogene, Boston, MA, USA, diluted 1:48,000) in GPB for 24 h, (5) biotin-conjugated donkey antirabbit IgG (Santa Cruz Biotechnology, Inc., Santa Cruz, CA, diluted 1:400) in GPB for 2 h, and (6) avidin-biotinylated HRP-complex (ABC, Vector Laboratories, Inc., Burlingame, CA) for 30 min. Fos immunoreactivity was then visualized as a black nuclear precipitate by means of a glucose oxidase-based nickel-intensified diaminobenzidine (Nickel-DAB) procedure.

After staining the Fos protein with Nickel-DAB, the free-floating sections were first washed with 0.1 M acetate buffer (pH 6.0) and then incubated for 24 h with a rabbit polyclonal antibody against tyrosine hydroxylase (Chemicon, Temecula, CA, USA, diluted 1:5000) in GPB. The sections were treated with biotin-conjugated donkey antimouse IgG (Santa Cruz Biotechnology, Inc.) diluted 1:400 in GPB for 2 h, then further incubated with avidin-biotinylated HRP-complex (ABC, Vector Laboratories, Inc.) for 30 min. Finally, the sections were visualized as a brown cytoplasmic precipitate using a diaminobenzidine procedure. Sections incubated without primary antibodies remained virtually free of immunolabeling. After processing, the sections were mounted and examined by light microscopy. The C1/C2 regions are mainly located in the rostral part of the area postrema (AP) [11], whereas the A1/A2 regions are localized more in the caudal part than C1/C2 [10], so we divided both the C1/C2 and the A1/A2 region into rostral and caudal parts to AP. The two to three sections containing the A1/A2 (−13.7 to −13.1 mm from the bregma) and the parvocellular part of the paraventricular nucleus (pPVN) (−1.9 mm from the bregma) that most closely matched the Paxinos and Watson [17] rat brain stereotaxic atlas and our previous study [20] were counted for each animal. All Fos- and/or TH-positive cells in both sides of each nuclear area were counted by staff blind to treatment. To avoid double counting, only neurons with a complete nucleus were counted.

All data shown are expressed as mean ± S.E. The comparisons between different groups were performed using one-way ANOVA followed by *Scheffé's post hoc* test. Brain areas showing between-group variations with $p < 0.05$ were regarded as statistically significant.

Concentrations of blood lactate after 30 min of running were 1.58 ± 0.08 mmol/l in the controls ($n = 4$), 1.71 ± 0.08 mmol/l in the below-LT running ($n = 5$), and 3.34 ± 0.06 mmol/l in the supra-LT running group ($n = 5$). Running-induced increase in plasma ACTH concentrations in the control ($n = 4$), below-LT ($n = 5$), and supra-LT running groups ($n = 5$) were 108 ± 17, 177 ± 52 and 473 ± 77 pg/ml, respectively. Values are expressed as mean ± S.E. These absolute values were consistent with our previous results [21]. Blood lactate and plasma ACTH concentrations significantly increased in supra-LT running groups compared to controls and below-LT running groups (one-way ANOVA followed by *Scheffé's post hoc* test, $p < 0.01$ versus control and below-LT running groups). The photomicrographs in Fig. 1 show TH- and/or Fos-ir cell labeling in the A1/A2 (Fig. 1A–F), and Fos-ir cell labeling in the pPVN (Fig. 1G–I) in supra/below-LT running and control animals. In the A1/A2, as revealed in the quantitative data, labeling is minimal in the controls (Fig. 1A and D). Increased running speed increased the number of TH/Fos-ir cells in both nuclei. Supra-LT running markedly increased the cell number of TH/Fos-ir cells in both the A1 cell group (Fig. 1C) and the A2 cell group (Fig. 1F) as expected. It is of interest that below-LT running also increased the cell number of TH/Fos-ir cells in both the A1 cell group (Fig. 1B) and the A2 cell group (Fig. 1E),

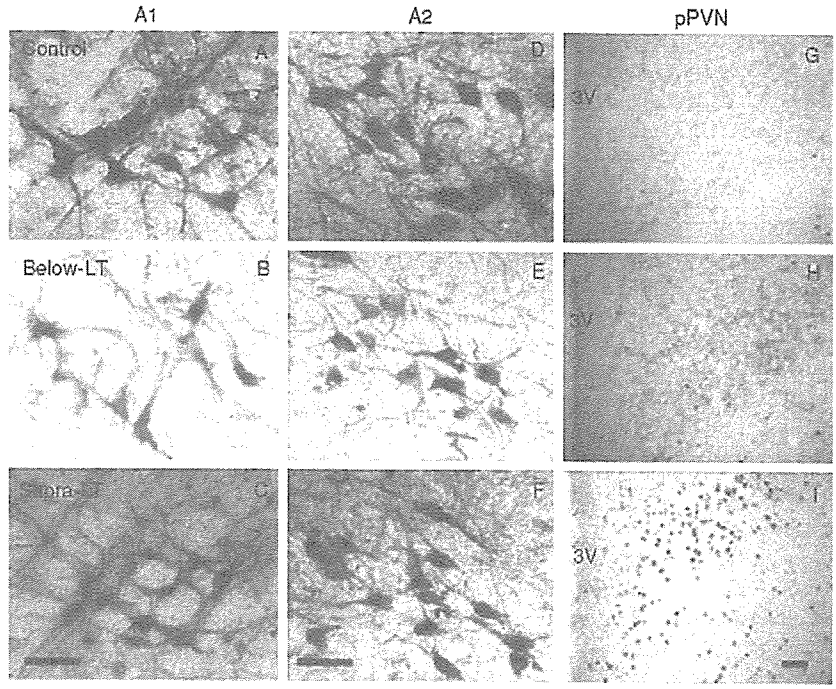

Fig. 1. Photomicrographs show double immunostaining with TH/Fos-ir and Fos-ir cells in the A1 (A–C), A2 (D–F) and the pPVN (G–I) of rats subjected to treadmill running at 0 m/min (controls: A, D and G), 15 m/min (below-LT running: B, E and H), and 25 m/min (supra-LT running: C, F and I). TH/Fos-ir cells were gradually labeled in response to the exercise intensity, whereas Fos-ir cells were remarkably labeled only Supra-LT running in the pPVN. TH-ir cells and Fos-ir cells were stained brown and black, respectively. Scale bars = 50 μm.

although the extent of accumulation was smaller than that for supra-LT running. Supporting our previous study [21], supra-LT (Fig. 1I) running markedly increased the number of Fos-ir cells in the pPVN, whereas control (Fig. 1G) and below-LT (Fig. 1H) running increased them to a lesser extent. The percentage of c-Fos expression in the TH-ir cells of the A1 and the A2 cell groups significantly increased according to running speed. The increased percentages of TH/Fos-ir cells were statistically different among the control, below-LT, and supra-LT running groups (one-way ANOVA followed by *Scheffé's post hoc* test, $p < 0.01$) (Fig. 2A). The number of Fos-ir cells in the pPVN was significantly higher than those in the below-LT and the control groups (one-way ANOVA followed by *Scheffé's post hoc* test, $p < 0.01$ versus control and below-LT running groups) (Fig. 2B).

The running protocol in this study consisted of both below- and supra-LT running, which are typical exercise intensities that induce different metabolic and cardiovascular responses to running, as conclusively established in humans [1] and rats [2,24]. In our running model used in this study, rats subjected to running at supra-LT showed a significant increase in plasma ACTH levels and osmolality together with blood lactate levels, while rats in the below-LT running group did not [20,25]. Indeed, the fact that blood lactate and plasma ACTH concentrations and the number of Fos-ir cells in the pPVN were significantly elevated in the supra-LT running group demonstrates the validity and reproducibility of our running model as used in the present study. Our running model consists of two different runs with or without stress response.

TH/Fos-ir cells markedly increased in the A1/A2 at supra-LT running as shown in Figs. 1 and 2. The A1/A2 noradrenergic neurons showed the most prominent activation in supra-LT running, suggesting that these NA neurons play a crucial role in

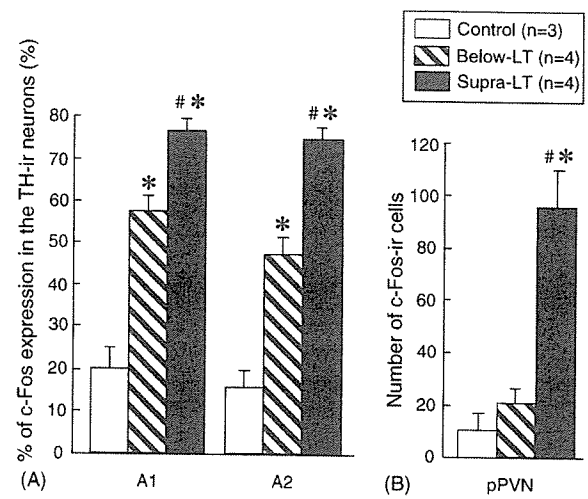

Fig. 2. Percentage of c-Fos expression in TH-ir cells in the A1/A2 (A) and number of Fos-ir cells in the pPVN (B) for the control (open bars), the below-LT (stripe bars) and the supra-LT (filled bars) groups. The supra-LT running markedly increased the number of Fos/TH-ir cells in the A1/A2, and the percentage of c-Fos expression in the TH-ir cells of the A1/A2 significantly increased according to running speed (A). Fos-ir cells in the pPVN significantly increased in supra-LT running (B). Values are mean ± S.E. $^{*}p < 0.05$ vs. control. $^{\#}p < 0.01$ vs. below-LT (*Scheffé's post hoc* tests) ($n = 3$–4).

some physiological events induced by running stress, for example, the pPVN receives dense projections from the A1/A2 [21], and it has been reported that both nuclei involve several stress responses [3,4,16,23], including swimming stress [22]. Furthermore, we delineated anatomical activation of the pPVN where it receives NA innervation during supra-LT running [20], suggesting that the A1/A2 play a provocative role in regulating ACTH release in running stress.

We also have demonstrated that running stress causes plasma hyper-osmolality, resulting in the activation of hypothalamic arginine–vasopressin (AVP) neurons in the pPVN and the SON [20]. Because NA neurons in the A1 enhance responsiveness to plasma hyper-osmolality in the PVN neurosecretory cells [27], activation of hypothalamic AVP neurons during running stress that induces plasma hyper-osmolality might be amplified by these NA neurons.

Unexpectedly, TH/Fos-ir cells in the A1/A2 also showed a significant increase in below-LT running (running without ACTH release), unlike the pPVN. The reason why below-LT running increased TH/Fos-ir cells in the A1/A2 is unclear at present. However, one possible involvement appears to exist. In contrast, only in the stress response induced above the LT did the cardiovascular response increase linearly with running speed [1,24]. Since these areas are generally accepted as being the circulation center in the brain stem [19] and A1/A2 neurons are responsive to different cardiovascular conditions [14], it is possible that A1/A2 are activated in response to the cardiovascular response during below-LT running. It is not known why below-LT running increased TH/Fos-ir cells in the A1/A2 without activation of the pPVN; however, the pPVN may receive GABAergic inhibitory inputs from other brain areas, such as the bed nucleus of the stria terminalis [5,9] or hippocampal formation [8], suggesting involvement of another inhibitory factors that regulate running-induced ACTH release.

The physiological role of activated NA neurons in the A1/A2 could not be determined in this study; however, we first demonstrated anatomical evidence that these neurons are responsive not only to supra-LT running, but also to below-LT running. This is to be expected in regulatory systems that respond to running. Neuroendocrine systems in the hypothamalo-pituitary-adrenal axis and sympathetic nervous system including cardiovascular regulation, act cooperatively to support the increased metabolic demands made by contracting muscles when running speed increases [7]. The A1/A2 noradrenergic neurons may be involved in the regulation of both systems. Further studies are needed, using adrenoreceptor antagonists and agonists or by means of lesion studies, to estimate the physiological contributions of these neurons during running.

In summary, TH-containing neurons in the A1/A2 are linearly activated with exercise intensity. We thus suggest that these neurons are activated in response not only to running stress and other types of stress, but also to other physiological responses enhanced by non-stressful running (running without ACTH release). These findings will be helpful in studies of specific neurocircuits and in identifying their functions in response to running at different intensities.

References

[1] R.M. Berne, M.N. Levy, Cardiovascular Physiology, fifth ed., C.V. Mosby Company, 1986.

[2] G.A. Brooks, T.P. White, C.M. Donovan, G.A. Gaesser, Determination of metabolic and heart rate responses of rats to treadmill exercise, J. Appl. Physiol. 45 (1978) 1009–1015.

[3] D.N. Darlington, J. Shinsako, M.F. Dallman, Medullary lesions eliminate ACTH responses to hypotensive hemorrhage, Am. J. Physiol. 251 (1986) R106–R115.

[4] C.V. Dayas, K.M. Buller, J.W. Crane, Y. Xu, T.A. Day, Stressor categorization: acute physical and psychological stressors elicit distinctive recruitment patterns in the amygdala and in medullary noradrenergic cell groups, Eur. J. Neurosci. 14 (2001) 1143–1152.

[5] J.D. Dunn, Plasma corticosterone responses to electrical stimulation of the bed nucleus of the stria terminalis, Brain Res. 407 (1987) 327–331.

[6] P.A. Farrell, T.L. Garthwaite, A.B. Gustafson, Plasma adrenocorticotropin and cortisol responses to submaximal and exhaustive exercise, J. Appl. Physiol. 55 (1983) 1441–1444.

[7] H. Galbo, The hormonal response to exercise, Diabetes Metab. Rev. 1 (1986) 385–408.

[8] J.P. Herman, W.E. Cullinan, Neurocircuitry of stress: central control of the hypothalamo-pituitary-adrenocortical axis, Trends Neurosci. 20 (1997) 78–84.

[9] J.P. Herman, W.E. Cullinan, S.J. Watson, Involvement of the bed nucleus of the stria terminalis in tonic regulation of paraventricular hypothalamic CRH and AVP mRNA expression, J. Neuroendocrinol. 6 (1994) 433–442.

[10] M. Kalia, K. Fuxe, M. Goldstein, Rat medulla oblongata. II. Dopaminergic, noradrenergic (A1 and A2) and adrenergic neurons, nerve fibers, and presumptive terminal processes, J. Comp. Neurol. 233 (1985) 308–332.

[11] M. Kalia, K. Fuxe, M. Goldstein, Rat medulla oblongata. III. Adrenergic (C1 and C2) neurons, nerve fibers and presumptive terminal processes, J. Comp. Neurol. 233 (1985) 333–349.

[12] A. Luger, P.A. Deuster, P.W. Gold, D.L. Loriaux, G.P. Chrousos, Hormonal responses to the stress of exercise, Adv. Exp. Med. Biol. 245 (1988) 273–280.

[13] W.P. Morgan, Affective beneficence of vigorous physical activity, Med. Sci. Sports Exerc. 17 (1985) 94–100.

[14] A.Z. Murphy, M. Ennis, M.T. Shipley, M.M. Behbehani, Directionally specific changes in arterial pressure induce differential patterns of fos expression in discrete areas of the rat brainstem: a double-labeling study for Fos and catecholamines, J. Comp. Neurol. 349 (1994) 36–50.

[15] K. Pacak, Stressor-specific activation of the hypothalamic–pituitary–adrenocortical axis, Physiol. Res. 49 (2000) S11–S17.

[16] K. Pacak, M. Palkovits, R. Kvetnansky, G. Yadid, I.J. Kopin, D.S. Goldstein, Effects of various stressors on in vivo norepinephrine release in the hypothalamic paraventricular nucleus and on the pituitary–adrenocortical axis, Ann. N.Y. Acad. Sci. 771 (1995) 115–130.

[17] G. Paxinos, C. Watson, The Rat Nervous System, second ed., Academic Press, 1998.

[18] P. Rahkila, E. Hakala, M. Alen, K. Salminen, T. Laatikainen, Beta-endorphin and corticotropin release is dependent on a threshold intensity of running exercise in male endurance athletes, Life Sci. 43 (1988) 551–558.

[19] D.A. Ruggiero, S.L. Cravo, V. Arango, D.J. Reis, Central control of the circulation by the rostral ventrolateral reticular nucleus: anatomical substrates, Prog. Brain Res. 81 (1989) 49–79.

[20] T. Saito, H. Soya, Delineation of responsive AVP-containing neurons to running stress in the hypothalamus, Am. J. Physiol. Regul. Integr. Comp. Physiol. 286 (2003) R484–R490.

[21] P.E. Sawchenko, L.W. Swanson, Central noradrenergic pathways for the integration of hypothalamic neuroendocrine and autonomic responses, Science 214 (1981) 685–687.

[22] A.J. Scheurink, A.B. Steffens, R.P. Gaykema, Paraventricular hypothalamic adrenoceptors and energy metabolism in exercising rats, Am. J. Physiol. 259 (1990) R478–R484.

[23] D.W. Smith, K.M. Buller, T.A. Day, Role of ventrolateral medulla catecholamine cells in hypothalamic neuroendocrine cell responses to systemic hypoxia, J. Neurosci. 15 (1995) 7979–7988.
[24] B. Sonne, H. Galbo, Simultaneous determinations of metabolic and hormonal responses, heart rate, temperature and oxygen uptake in running rats, Acta Physiol. Scand. 109 (1980) 201–209.
[25] H. Soya, Stress response to exercise and its hypothalamic regulation: Role of arginine–vasopressin in exercise, nutrition and environmental stress, Cooper Publishing, 2001, pp. 21–37.
[26] H. Tanaka, M. Shindo, The benefits of the low intensity training, Ann. Physiol. Anthropol. 11 (1992) 365–368.
[27] J. Tanaka, M. Nomura, H. Saito, Noradrenergic inputs enhance the response of neurosecretory cells to osmotic stimulation, Neuroreport 3 (1992) 256–258.
[28] S.P. von Duvillard, Exercise lactate levels: simulation and reality of aerobic and anaerobic metabolism, Eur. J. Appl. Physiol. 86 (2001) 3–5.

Original article

Nuclear Medicine Communications

Gender difference in brain perfusion ^{99m}Tc-ECD SPECT in aged healthy volunteers after correction for partial volume effects

Zhi-Jie Li[a,c], Hiroshi Matsuda[a], Takashi Asada[b], Takashi Ohnishi[a], Hidekazu Kanetaka[a], Etsuko Imabayashi[a] and Fumiko Tanaka[a]

Background Previous reports have yielded controversial results concerning gender differences in regional cerebral blood flow (rCBF). To elucidate this issue, we compared ^{99m}Tc ethyl cysteinate dimer single photon emission computed tomography (SPECT) images for brain perfusion between aged-matched healthy men and women after correction for partial volume effects (PVEs).

Methods Brain perfusion SPECT in the resting state was performed on 40 healthy, right-handed subjects, 20 men and 20 women, with an age range of 58–86 years, who did not differ sociodemographically. PVE correction was performed using grey matter volume measured by magnetic resonance imaging. Statistical parametric mapping was used for the analysis of the adjusted rCBF images of relative flow distribution.

Results The PVE correction revealed that women had higher rCBF in left inferior frontal gyrus, bilateral middle temporal gyri, and left superior temporal gyrus. Men had higher rCBF in left superior frontal gyrus, right medial frontal gyrus, right superior parietal lobule, right postcentral gyrus, right cerebellum, right middle frontal gyrus, right fusiform gyrus, and right precuneus.

Conclusion Significant gender differences in rCBF existed in these healthy volunteers. The PVE correction of SPECT images revealed gender differences that were consistent with the universal findings of better performance on verbal tasks in women and on visuospatial tasks in men. *Nucl Med Commun* 25:999–1005 © 2004 Lippincott Williams & Wilkins.

Nuclear Medicine Communications 2004, 25:999–1005

Keywords: single photon emission computed tomography, ^{99m}Tc ethyl cysteinate dimer, regional cerebral blood flow, gender

[a]Department of Radiology, National Center Hospital for Mental, Nervous, and Muscular Disorders, National Center of Neurology and Psychiatry, Tokyo, [b]Department of Neuropsychiatry, Institute of Clinical Medicine, University of Tsukuba, Ibaraki and [c]Department of Nuclear Medicine, The Second Clinical Hospital of China Medical University, Shen-Yang City, China.

Correspondence to Dr Hiroshi Matsuda, Department of Nuclear Medicine, Saitama Medical School Hospital, 38 Morohongo Moroyama-machi, Iruma-gun, Saitama, 350-0495, Japan.
Tel: +81 49 276 1302; fax: +81 49 276 1301
e-mail: matsudah@saitama-med.ac.jp

Received 10 October 2003 Revised 18 March 2004
Accepted 25 March 2004

Introduction

Gender differences in behaviours such as cognitive and emotional processing are increasingly recognized. Such differences are considered to have biological substrates. Neuropsychological measures have demonstrated gender differences [1–3]. Functional neuroimaging techniques such as positron emission tomography (PET) and single photon emission computed tomography (SPECT) have also been used to observe the gender differences in regional cerebral blood flow (rCBF) or regional cerebral metabolic rate for glucose (rCMRglc) quantitatively or semiquantitatively [3–13], but at present the findings are controversial. Although some studies indicated that gender differences exist in both rCBF and rCMRglc, the regions focused on in the various studies were not entirely consistent. Nevertheless, others reported no gender based differences [5,6]. Many factors are likely to have contributed to these discrepancies, including differences in the normal subjects selected, tracers and scanners, and methods of analysis. One possible explanation is an interaction between a subject's age and gender, because studies reported that differences between the sexes occur in younger cohorts only and become less prominent in later years [14–16]. Further, even when gender differences are observed, it is still unclear whether the differences in PET or SPECT imaging between women and men reflect true gender differences of rCBF or rCMRglc. Due to the limited spatial resolution of PET or SPECT, the accurate measurement of tracer concentration in brain structures depends on several physical limitations, particularly the relation between object size and scanner spatial resolution. This relation, known as the partial volume effect (PVE), biases the measured concentration in small structures by diminishing the true concentration. The PVE causes a volume averaging effect between the tissue elements of grey matter, white matter, and cerebrospinal fluid in a region of the brain. Since the results of magnetic resonance imaging (MRI)

studies have demonstrated gender related differences in brain morphology [17,18], PVE may exert an influence on PET and SPECT results. Van Laere and Dierckx [13] considered the regional structure of the brain tissue when they studied gender differences, but used an indirect method, comparing the grey matter volume and brain perfusion. No voxel based PVE correction was done in the gender difference study with PET or SPECT. Recently, the high-resolution anatomical detail available with MRI techniques has led to the development of magnetic resonance based methods to correct PET or SPECT data for PVE [19–24]. In the present research our aim was to investigate the gender difference in aged healthy volunteers using brain perfusion SPECT imaging and to determine which brain structures show a greater influence of PVE correction.

Methods

Study population

A sample of 40 right handed healthy adults, 20 women and 20 men, with an age range of 58–86 years was recruited from spouses of patients with Alzheimer's disease who were referred to the memory clinic of our hospital. These healthy aged subjects were known not to have cognitive changes during the follow-up period of more than 2 years since these spouses were attendant for the patients. They had no neurological or psychiatric disorders, including alcoholism, substance abuse, atypical headache, head trauma with loss of consciousness, or asymptomatic cerebral infarction detected by T2 weighted MRI. Women and men did not differ socio-demographically; age (mean ± SD), women 68.4 ± 7.4, men 72.4 ± 7.5; education, women 13.0 ± 2.2, men 13.8 ± 2.0; verbal IQ [25], women 117.9 ± 9.1, men 121.2 ± 6.9; performance IQ, women 114.3 ± 9.3, men 110.7 ± 9.3; total IQ, women 117.4 ± 8.1, men 117.6 ± 6.8; two-sample *t*-test, all two-tailed $P > 0.3$. There were no significant differences between men and women in the Mini-Mental State Examination [26]: women 29.3 ± 0.9, men 28.6 ± 1.4, and scores of Wechsler memory scales (revised) [27], either. The ethics committee of our centre approved this study for healthy volunteers, all of whom gave their informed consent to participate.

SPECT study and PVE correction

Before SPECT was performed, an intravenous line was established in all subjects. They were injected while lying down in the supine position with eyes closed in a dimly lit, quiet room. Each received a 600 MBq intravenous injection of ^{99m}Tc ethyl cysteinate dimer (^{99m}Tc-ECD). Ten minutes after the injection of ^{99m}Tc-ECD, brain SPECT was performed using a triple-head SPECT system (Multispect 3; Siemens Medical Systems Inc., Hoffman Estates, IL) equipped with high-resolution fanbeam collimators. For each camera, projection data were obtained in a 128 × 128 format for 24 angles of 120° at 50 s per angle. A Shepp and Logan Hanning filter was used as a filtered back-projection method for SPECT image reconstruction at 0.7 cycle/cm. Attenuation correction was performed using Chang's method with an optimized effective attenuation coefficient of 0.09 cm^{-1}.

Correction for PVE was performed for atrophy correction in SPECT images using three dimensional volumetric T1 weighted magnetic resonance (MR) images (a 1.0 T system; Magnetom Impact Expert, Siemens, Erlagen, Germany) as described in previous studies [23,24]. A three-dimensional volumetric acquisition of a T1 weighted gradient-echo sequence produced a gapless series of thin sagittal sections using a magnetization preparation rapid acquisition gradient-echo sequence (TE/TR, 4.4/11.4 ms; flip angle, 15°; acquisition matrix, 256 × 256; slice thickness, 1.23 mm). The MR images acquired were reformatted to gapless 2 mm thick transaxial images. Then MR images were converted to the same isometric matrix size as that for SPECT images. Then Statistical Parametric Mapping 99 (SPM99, www.fil.ion.bpmf.ac.uk/spm/) segmented these isometric MR images into grey matter, white matter, cerebrospinal fluid, and other compartments. The segmentation procedure involves calculating, for each voxel, a Bayesian probability of belonging to each tissue class based on *a priori* MRI information with inhomogeneity correction for the magnetic field. The Automated Image Registration (AIR) software (www.loni.ucla.edu/NCRR/Software/AIR.htm) was used to align the SPECT to the MRI scans of each subject using a six-parameter rigid-body transformation. Prior to co-registration of SPECT and MRI, the outer scalp was removed from MRI by applying a binary mask for the whole brain mentioned later to the MRI. A three-dimensional convolution with the point spread function of the SPECT device (assumed to be a simple three dimensional Gaussian with full width at half maximum (FWHM) of 9.0 × 9.0 × 9.0 mm), was performed to obtain coefficients of dispersion for each voxel. This procedure of identification of spatial resolution between grey matter SPECT and MR images makes it possible to correct PVE by division of these two images in the final procedure. These convoluted grey matter and white matter images were normalized to have a maximum count of 1.0 as 32 bit real values. A binary volume image was created from this convoluted grey matter image with the threshold set to 35% of the maximum value as a mask image for grey matter. A mask image for the whole brain was created from this mask image for grey matter by filling the interior holes in the brain. Then white matter SPECT images were simulated from these normalized white matter MR images with convolution as follows. The maximum count of 1.0 for the normalized white matter MR image was replaced by the maximum SPECT count in the white matter. To get the maximum count for the white matter of SPECT, a region of interest (ROI) was automatically determined by setting the threshold to

above 95% of the maximum count density of the white matter MR images. The grey matter SPECT images were obtained by subtraction of these white matter SPECT images from the original SPECT images co-registered to MRI. Last, the grey matter SPECT image was divided by the normalized grey matter MR image with equivalent spatial resolution to SPECT on a voxel-by-voxel basis. The mask image for grey matter was applied to this divided image. In the present study, a fully automated program for the PVE correction was developed using C + + language.

Image formatting and analysis

All subsequent image manipulation and data analysis were performed on a personal computer with an operating system of Windows XP. Grey matter SPECT images before and after atrophy correction and convoluted grey matter images segmented from MRI were spatially normalized in SPM99 to a standardized stereotactic space based on the Talairach and Tournoux atlas [28], using 12-parameter linear affine normalization and further 12 non-linear iteration algorithms with an original template for ^{99m}Tc-ECD [29] and with a template for *a priori* grey matter of SPM99 respectively. Then, images were smoothed using a 12 mm FWHM isotropic Gaussian kernel. The initial parameters of the image matrix were $128 \times 128 \times n$, where n is the number of slices covering the whole brain. The final image format is 16-bit, with a matrix size of $79 \times 95 \times 68$ and a voxel size $2 \times 2 \times 2$ mm.

Data sets were handled with SPM99. Women and men were compared using the 'compare population one scan/subject' routine, which carries out a fixed effects simple t-test for each voxel. The 'proportional scaling' routine was used to control for individual variation in global ^{99m}Tc-ECD uptake; these data will be referred to as 'adjusted rCBF.' The grey matter threshold was set at 80% of whole brain mean. Gender differences in grey matter concentration were also examined using voxel based morphometry as described in a previous study [30]. The resulting set of values for each contrast constituted a statistical parametric map of the t statistic SPM$\{t\}$. The SPM$\{t\}$ maps were then transformed to the units of normal distribution (SPM$\{Z\}$), and height threshold was set to $P < 0.005$ with cluster extent $K > 100$ voxels. Anatomical localization was according to Talairach coordinates, obtained from Brett's transformations (www.mrc-cbu.cam.ac.uk/Imaging/mnispace.html).

Results

Spatially normalized SPECT images for average in 20 healthy men and 20 healthy women were shown before and after PVE correction in Fig. 1. The PVE correction made the rCBF distribution more homogenous than the original distribution.

Before PVE correction, women showed higher perfusion in left superior temporal gyrus and left supramarginal gyrus than men. On the other hand, men showed higher perfusion in right medial frontal gyrus, bilateral middle frontal gyri, right fusiform gyrus, and right cerebellum than women (Fig. 2, Table 1).

After PVE correction, women showed higher perfusion in left inferior frontal gyrus, bilateral middle temporal gyri, and left superior temporal gyrus than men. Meanwhile, men showed higher perfusion in left superior frontal gyrus, right medial frontal gyrus, right superior parietal lobule, right postcentral gyrus, right cerebellum, right middle frontal gyrus, right fusiform gyrus, and right precuneus than women (Fig. 2, Table 1).

Women showed larger grey matter volume in left superior temporal gyrus than men (Fig. 3, Table 2). Meanwhile men showed larger grey matter volume in bilataral superior frontal gyri, bilateral medial frontal gyri, and left precentral gyrus than women (Fig. 3, Table 2).

Discussion

Although several investigators have examined gender differences in healthy volunteers using PET or SPECT, the findings of these studies have been inconsistent and controversial. In the present SPECT study we investigated gender differences in the relative distribution of brain perfusion and moreover examined the modifications that occur after correction for PVE. Totally significant gender differences in rCBF were noted in the present study, with PVE correction found to mostly influence frontal and parietal lobes.

A consistent finding in gender differences in behaviours is that women perform better than men on some verbal tasks [2]. Women tend to perform better on verbal learning and recall tasks [3]. The present correction for PVE compensated for the lower spatial resolution of SPECT compared with PET and possibly increased sensitivity in detecting rCBF differences between women and men. Although there is no reason why a region that performs differently under activation should have different perfusion at rest, the present results after PVE correction were more in line with a verbal fluency test which involved frontal areas than were results before PVE correction. Audenaert *et al.* [31] found that the activation paradigm of verbal fluency using SPECT caused a rCBF increase in left inferior frontal gyrus.

Moreover, PVE correction of SPECT images led to greater similarity of the present results to previously reported results using PET in which women showed higher resting rCBF in bilateral mid-temporal regions [7]. The finding of higher rCBF in women than in men disappeared after PVE correction in a supero-posterior

Fig. 1

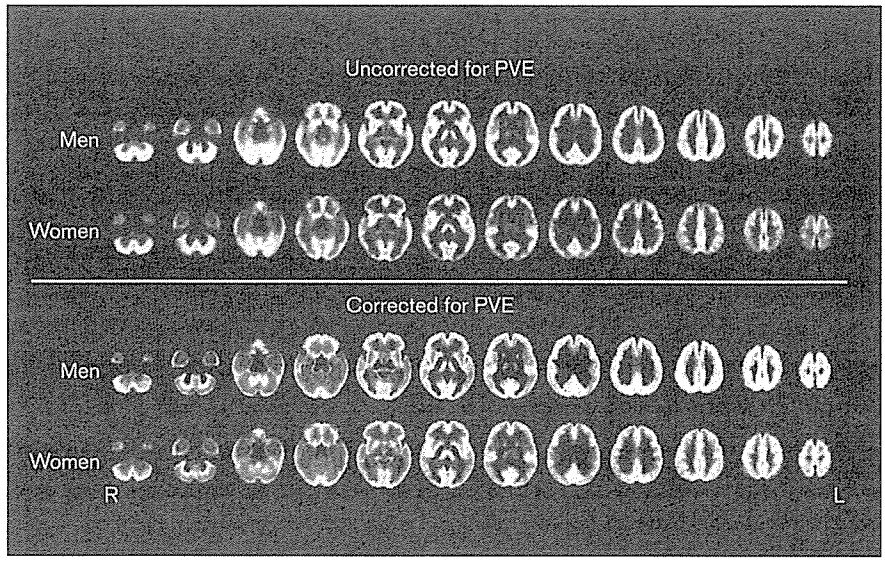

Spatially normalized SPECT images, as an average, in 20 healthy men and 20 healthy women before and after correction for partial volume effects (PVEs). Note the more homogenous distribution of regional cerebral blood flow (rCBF) after PVE correction.

Fig. 2

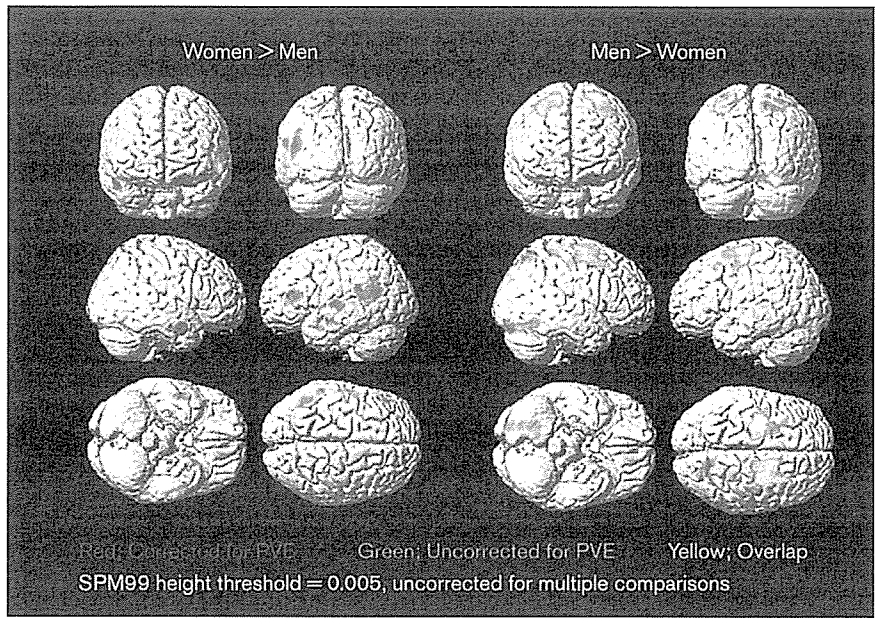

SPM99 results for differences of adjusted rCBF between healthy men and women before and after PVE correction. Dual colour display on surface rendered images of the standard MRI scans of significant gender differences (height threshold $P<0.005$, uncorrected for multiple comparisons) of adjusted rCBF before correction of PVEs as green and those of adjusted rCBF after PVE correction as red in aged healthy volunteers by SPM99. Overlapping areas are shown as yellow. (Abbreviations as in the legend to Fig. 1).

part of the left superior temporal gyrus and left supramarginal gyrus. This may result from increased grey matter volume in the left superior temporal gyrus in women as shown in Fig. 3.

Another consistent finding in gender differences in behaviours is that men excel in certain visuospatial tasks [1]. In the present study, PVE correction revealed that men had higher adjusted rCBF in right parietal lobes and

Table 1 **Gender differences in brain perfusion SPECT before and after PVE correction**

SPECT	Region	Brodmann area	Talairach coordinate			*Z* score
			x	*y*	*z*	
SPECT uncorrected for PVE						
Women>men	Left superior temporal gyrus	22	−44	−55	18	4.03
	Left superior temporal gyrus	21	−57	−10	−1	3.16
	Left supramarginal gyurs	39	−44	−55	32	3.08
Men>women	Right medial frontal gyrus	6	14	5	57	4
	Left middle frontal gyrus	6	−28	−7	54	3.81
	Right fusiform gyrus	19	24	−82	−13	3.67
	Right middle frontal gyrus	6	28	−1	52	3.56
	Right cerebellum (posterior lobe)		26	−57	−11	3.1
SPECT corrected for PVE						
Women>men	Right middle temporal gyrus	21	51	−1	−20	3.5
	Left inferior frontal gyrus	46	−50	33	9	3.29
	Left superior temporal gyrus	22	−53	2	−3	3.16
	Left middle temporal gyrus	21	−59	−8	−13	3.02
Men>women	Left superior frontal gyrus	6	−28	−8	63	3.97
	Right medial frontal gyrus	6	14	5	57	3.54
	Right superior parietal lobule	7	14	−61	58	3.53
	Right postcentral gyrus	3	30	−32	57	3.43
	Right cerebellum (posterior lobe)		8	−59	−11	3.37
	Right middle frontal gyrus	6	28	1	53	3.23
	Right fusiform gyrus	19	24	−74	−13	3.1
	Right precuneus	7	26	−73	53	3.03

right fusiform gyrus than women. Although, again, we have to be careful about linking rCBF differences at rest to those under activation, the present resting results after PVE correction more closely resembled the activation results in a visuospatial perception test [32] which involved the right parietal cortex and occipitotemporal junction than did results before PVE correction. Jones *et al.* [11] and Van Laere *et al.* [12] reported similar gender differences in adjusted rCBF of parietal lobes except that in their SPECT studies the direction of the differences was reversed, with women having higher resting rCBF in bilateral parietal lobes than men. Premotor and prefrontal cortices into which long association fibres project from the parietal cortex were also activated in a paradigm of visuospatial perception in a PET study [33]. In spite of larger grey matter volume in premotor and prefrontal cortices in men than in women as shown in Fig. 3, rCBF in these areas still remained higher in men than in women after PVE correction.

By using SPECT, Van Laere and Dierckx [13] found that men had relatively higher resting rCBF in the cerebellum than women. When they compared the perfusion with the grey matter volume measured by MRI, such a gender difference in perfusion was considered to be due to a gender difference in cerebellar volume. In contrast, the present study showed a consistent gender difference in the right cerebellum before and after PVE correction. Gur *et al.* [8] similarly found that men had relatively higher resting rCMRglc in bilateral cerebellar hemispheres compared with women. Volkow *et al.* [10] also reported similar significant differences in cerebellar metabolism between women and men, except that in their study the direction of the differences was reversed, with women having higher metabolism in bilateral cerebellar hemispheres, but none of the reports that mentioned gender differences in cerebellum clarified the detailed location in the cerebellum. In the present study, it is clear that only the right posterior cerebellum showed a gender difference before and after PVE correction. Conventionally, cerebellum is considered to be involved in motor function, but non-traditional roles for it in the regulation of autonomic function, behaviour and cognition are also recognized. As for the posterior lobe corresponding to neocerebellum, besides its role in coordinating extremity movement, non-motor functions, including modulation of thought, planning, strategy formation, spatial and temporal parameters, learning, memory and language have been proposed as well [34].

The discordant findings in gender differences in previous studies on PET or SPECT may be partly attributable to the substantial age differences in the groups studied. This may be particularly relevant for our group, since it included only post-menopausal women, and oestrogen has been considered to affect brain function [4,35]. Moreover, various degrees of brain atrophy among aged subjects would obscure true gender difference especially in a SPECT study with poorer resolution compared with PET. We believe that PVE correction is essential for detecting marginal gender differences in SPECT studies.

Finally, we must refer to the study limitations. First, we examined only the resting state and did not incorporate activation procedures. Thus, our conclusions concern topography of the human brain while it is idling, which

Fig. 3

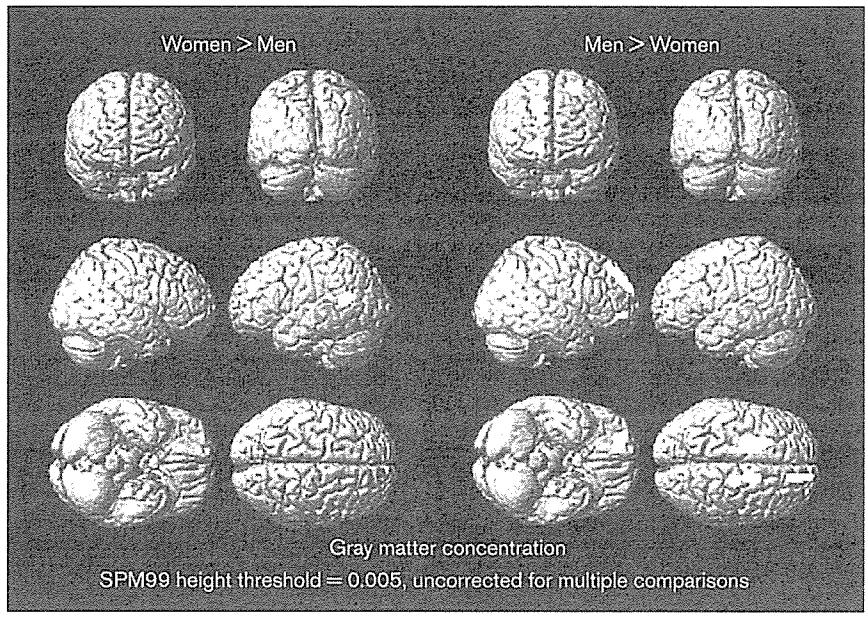

SPM99 results for differences of grey matter volume between healthy men and women. Grey scale display on surface rendered images of the standard MRI scans of significant gender differences (height threshold $P<0.005$, uncorrected for multiple comparisons) of grey matter volume in aged healthy volunteers by SPM99.

Table 2 Gender differences in grey matter volume

	Region	Brodmann area	Talairach coordinate			*Z* score
			x	*y*	*z*	
Women > men	Left superior temporal gyrus	22	−46	−56	16	3.92
Men > women	Right superior frontal gyrus	8	16	47	38	4.30
	Right medial frontal gyrus	10	14	48	−6	3.57
	Left superior frontal gyrus	6	−18	5	55	3.52
	Left medial frontal gyrus	6	−16	−17	56	3.12
	Left precentral gyrus	44	−44	12	12	2.77

may itself influence regional brain activity. Further gender differences may become evident when activity is measured during the performance of behavioural tasks. Nonetheless, measures of resting rCBF support a neurobiological explanation of some gender related differences in behaviour. Second, although the previous phantom study validated the present method for PVE correction, this correction is sensitive to errors, particularly image segmentation and image registration. Therefore we do not totally deny that the differences seen only after PVE correction can be artifacts induced by the correction method than true perfusion differences which were hidden by morphometric variations.

Conclusion

Gender effects on rCBF have not been consistent. Discrepancies among studies probably reflect multiple factors, including study conditions, subjects' characteristics, analysis strategies, and measurement variability. To investigate gender differences in resting rCBF, we focused our attention on correction for PVE in SPECT images of aged healthy women and men. The PVE correction disclosed significant gender differences in rCBF that agreed well with the consistent gender differences in behaviours of better performance noted on verbal tasks in women and on visuospatial tasks in men. Gender differences in grey matter volume agreed less with these gender differences in behaviours than rCBF after PVE correction. This PVE correction may be very helpful in SPECT studies on atrophied brain.

Acknowledgements

We thank the technologists at our hospital for data acquisition and Mr John Gelblum for proofreading this manuscript.

References

1 McGlone J, Kertesz A. Sex differences in cerebral processing of visuospatial tasks. *Cortex* 1973; **9**:313–320.

2 Kimura D, Harsham RA. Sex differences in brain organization for verbal and non-verbal functions. *Prog Brain Res* 1984; **61**:423–441.

3 Ragland JD, Coleman AR, Gur RC, Glanhn DC, Gur RE. Sex differences in brain–behavior relationships between verbal episodic memory and resting regional cerebral blood flow. *Neuropsychologia* 2000; **38**:451–461.

4 Baxter LR, Mazziotta JC, Phelps ME, Selin CE, Guze BH, Fairbanks L. Cerebral glucose metabolic rates in normal human females versus normal males. *Psychiatry Res* 1987; **21**:237–245.

5 Miura SA, Schapiro MB, Grady CL, Kumar A, Salerno JA, Kozachuk WE, *et al.* Effect of gender on glucose utilization rates in healthy humans: a positron emission tomography study. *J Neurosci Res* 1990; **27**:500–504.

6 Azari NP, Rapoport SI, Salerno JA, Grady CL, Gonzalez-Aviles A, Schapiro MB, *et al.* Gender differences in correlations of cerebral glucose metabolic rates in young normal adults. *Brain Res* 1992; **574**:198–208.

7 Andreason PJ, Zametkin AJ, Guo AC, Baldwin P, Cohen RM. Gender-related differences in regional cerebral glucose metabolism in normal volunteers. *Psychiatry Res* 1994; **51**:175–183.

8 Gur RC, Mozley LH, Mozley PD, Resnick SM, Karp JS, Alvai A, *et al.* Sex differences in regional cerebral glucose metabolism during a resting state. *Science* 1995; **267**:528–531.

9 Esposito G, Van Horn JD, Weinberger DR, Berman KF. Gender differences in cerebral blood flow as a function of cognitive state with PET. *J Nucl Med* 1996; **37**:559–564.

10 Volkow ND, Wang GJ, Fowler JS, Hitzemann R, Pappas N, Pascani K, Wong C. Gender differences in cerebellar metabolism: test–retest reproducibility. *Am J Psychiatry* 1997; **154**:119–121.

11 Jones K, Johnson KA, Becker JA, Spiers PA, Albert MS, Holman BL. Use of singular value decomposition to characterize age and gender differences in SPECT cerebral perfusion. *J Nucl Med* 1998; **39**:965–973.

12 Van Laere K, Versijpt J, Audenaert K, Koole M, Goethals I, Achten E, Dierckx R. ^{99m}Tc-ECD brain perfusion SPET: variability, asymmetry and effects of age and gender in healthy adults. *Eur J Nucl Med* 2001; **28**:873–887.

13 Van Laere KJ, Dierckx RA. Brain perfusion SPECT: age- and sex-related effects correlated with voxel-based morphometric findings in healthy adults. *Radiology* 2001; **221**:810–817.

14 Davis SM, Ackerman RH, Correia JA, Alpert NM, Chang J, Buonanno F, *et al.* Cerebral blood flow and cerebrovascular CO_2 reactivity in stroke-age normal controls. *Neurology* 1983; **33**:391–399.

15 Shaw TG, Mortel KF, Meyer JS, Rogers RL, Hardenberg J, Cutaia MM. Cerebral blood flow changes in benign aging and cerebrovascular disease. *Neurology* 1984; **34**:855–862.

16 Devous Sr. MD, Stokely EM, Chehabi HH, Bonte FJ. Normal distribution of regional blood flow measured by dynamic single-photon emission tomography. *J Cereb Blood Flow Metab* 1986; **6**:95–104.

17 Kertesz A, Polk M, Black SE, Howell J. Sex, handedness, and the morphometry of cerebral asymmetries on magnetic resonance imaging. *Brain Res* 1990; **530**:40–48.

18 Gur RC, Gunning-Dixon FM, Turetsky BI, Bilker WB, Gure RE. Brain region and sex differences in age association with brain volume. A quantitative MRI study of healthy young adults. *Am J Geriatr Psychiatry* 2002; **10**:72–80.

19 Mueller-Gaertner HW, Links JM, Prince JL, Bryan RN, McVeigh E, Leal JP, *et al.* Measurement of radiotracer concentration in brain gray matter using positron emission tomography: MRI-based correction for partial volume effects. *J Cereb Blood Flow Metab* 1992; **12**:571–583.

20 Labbe C, Froment JC, Kennedy A, Ashburner J, Cinotti L. Positron emission tomography metabolic data corrected for cortical atrophy using magnetic resonance imaging. *Alzheimer Dis Assoc Disord* 1996; **10**:141–170.

21 Meltzer CC, Zubieta JK, Brandt J, Tune LE, Mayberg HS, Frost JJ. Regional hypometabolism in Alzheimer's disease as measured by positron emission tomography after correction for effects of partial volume averaging. *Neurology* 1996; **47**:454–461.

22 Ibanez V, Pietrini P, Furey ML, Alexander GE, Millet P, Bokde AL, *et al.* Regional glucose metabolic abnormalities are not the result of atrophy in Alzheimer's disease. *Neurology* 1998; **50**:1585–1593.

23 Matsuda H, Kanetaka H, Ohnishi T, Asada T, Imabayashi E, Nakano S, *et al.* Brain SPET abnormalities in Alzheimer's disease before and after atrophy correction. *Eur J Nucl Med* 2002; **29**:1502–1505.

24 Matsuda H, Ohnishi T, Asada T, Li ZJ, Kanetaka H, Imabayashi E, *et al.* Correction for partial-volume effects on brain perfusion SPECT in healthy men. *J Nucl Med* 2003; **44**:1243–1252.

25 Wechsler D. *Wechsler Memory Scale–Revised, Manual.* New York: The Psychological Corporation; 1987. (Japanese edition by Nihon-bunkakagakusha; 2001, pp. 10–57.)

26 Folstein MF, Folstein SE, McHugh PR. Mini-Mental State: a practical method for grading the cognitive state of patients for the clinician. *J Psychiatr Res* 1975; **12**:189–198.

27 Wechsler D. *Wechsler Adult Intelligence Scale–Revised, Manual.* Cleveland, Ohio: The Psychological Corporation; 1981. (Japanese edition by Nihon-bunkakagakusha; 1990, pp. 69–128.)

28 Talairach J, Tournoux P. *Co-planar Stereotaxic Atlas of the Human Brain.* New York, NY: Thieme Medical; 1988, pp. 93–108.

29 Ohnishi T, Matsuda H, Hashimoto T, Kunihiro T, Hishikawa M, Uema T, Sasaki M. Abnormal regional cerebral blood flow in childhood autism. *Brain* 2000; **123**:1838–1844.

30 Ohnishi T, Matsuda H, Tabira T, Asada T, Uno M. Changes in brain morphology in Alzheimer disease and normal aging: Is Alzheimer disease an exaggerated aging process? *Am J Neuroradiol* 2001; **22**: 1680–1685.

31 Audenaert K, Brans B, Van Laere K, Lahorte P, Versijpt, van Heeringen K, Dierckx R. Verbal fluency as a prefrontal activation probe: a validation study using ^{99m}Tc-ECD brain SPET. *Eur J Nucl Med* 2000; **27**: 1800–1808.

32 Faillenot I, Decety J, Jeannerod M. Human brain activity related to the perception of spatial features of objects. *Neuroimage* 1999; **10**: 114–124.

33 Ghatan PH, Hsife JC, Wirsen-Meuriling A, Wredling R, Eriksson L, Stone-Elander S, *et al.* Brain activation induced by the perceptual maze test: A PET study of cognitive performance. *Neuroimage* 1995; **2**:112–124.

34 Afifi AK, Bergman RA. *Functional Neuroanatomy.* New York, NY: McGraw-Hill; 1998, pp. 326–327.

35 Joseph JA, Kochman K, Roth GS. Reduction of motor behavioral deficits in senescence via chronic prolactin or estrogen administration: time course and putative mechanisms of action. *Brain Res* 1989; **505**:195–202.

Superiority of 3-Dimensional Stereotactic Surface Projection Analysis over Visual Inspection in Discrimination of Patients with Very Early Alzheimer's Disease from Controls Using Brain Perfusion SPECT

Etsuko Imabayashi, MD[1,2]; Hiroshi Matsuda, MD[1]; Takashi Asada, MD[3]; Takashi Ohnishi, MD[1]; Shigeki Sakamoto, MD[1]; Seigo Nakano, MD[4]; and Tomio Inoue, MD[2]

[1]Department of Radiology, National Center Hospital for Mental, Nervous, and Muscular Disorders, National Center of Neurology and Psychiatry, Tokyo, Japan; [2]Department of Radiology, Yokohama City University School of Medicine, Yokohama, Japan; [3]Department of Neuropsychiatry, Institute of Clinical Medicine, University of Tsukuba, Ibaraki, Japan; and [4]Department of Geriatric Medicine, National Center Hospital for Mental, Nervous, and Muscular Disorders, National Center of Neurology and Psychiatry, Tokyo, Japan

In Alzheimer's disease (AD), regional cerebral blood flow (rCBF) in the posterior cingulate gyri and precunei has been reported to decrease even at a very early stage. It may be helpful to use statistical image analysis to distinguish slight decreases in rCBF in this area. We compared a 3-dimensional stereotactic surface projection (3D-SSP) technique with visual inspection in the discrimination of patients with very early AD from age-matched controls using brain perfusion SPECT. **Methods:** SPECT was obtained in 38 patients with probable AD at a very early stage and after a mean interval of 15 mo and in 76 age-matched healthy volunteers. We randomly divided these subjects into 2 groups. The first group was used to identify the areas with significant decreases of rCBF in patients compared with healthy control subjects based on the voxel-based analysis using 3D-SSP. The second group was used to compare the discrimination ability between patients and control subjects by 3D-SSP with that by visual inspection. In the second group, a *Z*-score map for a SPECT image of a subject was obtained by comparison with mean and SD SPECT images of control subjects for each voxel after anatomic standardization and voxel normalization to reference regions. Receiver operating characteristic (ROC) curves for a *Z*-score discriminating patients with AD from control subjects were analyzed in areas with significant decreases of rCBF identified in the first group. For visual inspection, 6 physicians graded the rCBF decrease on SPECT images for ROC curves. They inspected the images twice at an interval of >2 wk, and intra- and interobserver reliabilities were determined. **Results:** Visual inspection showed fair-to-excellent intra- and interobserver reliabilities. The 3D-SSP demonstrated an accuracy of 86.2% for discriminating patients with AD from control subjects when analyzing the posterior cingulate gyri and precunei with global mean normalization. In contrast, visual inspection did not show an accuracy of >74.0% for this discrimination. **Conclusion:** The ability of 3D-SSP to discriminate patients with very early AD from control subjects is superior to that of visual inspection. It is clinically useful and reliable to adopt the use of 3D-SSP as an adjunct to visual interpretation.

Key Words: Alzheimer's disease; SPECT; regional cerebral blood flow; 3-dimensional stereotactic surface projection

J Nucl Med 2004; 45:1450–1457

In a very early stage of Alzheimer's disease (AD), even before a clinical diagnosis of probable AD is possible, decreases in regional cerebral blood flow (rCBF) and glucose metabolism in the posterior cingulate gyri and precunei have been reported using PET (*1,2*) or SPECT (*3,4*). Pathologic degeneration of neurons in this area had already been reported in subjects with early AD before these neuroimaging findings became apparent (*5*). However, it is virtually impossible to distinguish a slight decrease of flow or metabolic activity in this area in subjects with early AD by visual inspection, since metabolic activity in the posterior cingulate cortex is as high as in the primary visual cortex in healthy individuals at rest (*2*). The fact that recent medications such as cholinesterase inhibitors delay the progression of AD (*6*) has increased the importance of diagnosis of AD at an earlier stage. Although recent advances in computer-assisted analysis of PET or SPECT images using 3-dimensional stereotactic surface projection (3D-SSP) (*1,2,7*) or statistical parametric mapping (SPM) (*4,8,9*) have made it

Received Aug. 9, 2003; revision accepted Jan. 28, 2004.

For correspondence or reprints contact: Hiroshi Matsuda, MD, Department of Radiology, National Center Hospital for Mental, Nervous, and Muscular Disorders, National Center of Neurology and Psychiatry 4-1-1, Ogawahigashi, Kodaira, Tokyo, 187-8551, Japan.

E-mail: matsudah@saitama-med.ac.jp

easier to detect these regional metabolic or perfusion changes, there have been few studies on the ability to discriminate early AD subjects from healthy volunteers using these stereotactic methods in the clinical setting. The purpose of our study was to compare a 3D-SSP analysis technique with visual inspection in the ability to discriminate very early AD subjects from healthy volunteers using brain perfusion SPECT.

MATERIALS AND METHODS

Subjects

We retrospectively chose 38 patients (16 men, 22 women) with a clinical diagnosis of probable AD according to the National Institute of Neurologic and Communicative Disorders and Stroke and the Alzheimer's Disease and Related Disorders Association criteria (NINCDS–ADRDA) (*10*). The patients ranged in age from 48 to 81 y, with a mean age ± SD of 71.1 ± 8.4 y. At the initial visit, they underwent thorough neuropsychologic testing (*11*) and showed selective impairment of delayed recall with no apparent loss in general cognitive, behavioral, or functional status (Table 1). They corresponded to the criteria of mild cognitive impairment (MCI) proposed by Petersen et al. (*12*) or 0.5 in Clinical Dementia Rating (*13*). Each patient underwent baseline brain perfusion SPECT at the time of the initial visit and was clinically followed-up with a second SPECT study at intervals ranging from 11.2 to 25.4 mo (mean, 15.0 mo). At the time of the baseline SPECT study, the Mini-Mental State Examination (MMSE) score (*14*) was 26.1 ± 1.6 (mean ± SD). The score significantly ($P < 0.05$; repeated measurement ANOVA with Dunnet test) decreased to 22.0 ± 3.7 at the time of the follow-up SPECT study. At the third neuropsychologic assessment without a SPECT study, except for forward and backward recall of digit span, all of the other assessments described in Table 1 were significantly ($P < 0.05$) decreased from the baseline study.

Seventy-six healthy volunteers (37 men, 39 women; age range, 67–87 y; mean age, 71.0 ± 7.1) were also studied. They had no neurologic or psychiatric disorders, including alcoholism, substance abuse, atypical headache, head trauma with loss of consciousness, or asymptomatic cerebral infarction detected by T2-weighted MRI. They did not significantly differ in age, sex, or education from the AD patients (Table 1). Spouses of the patients comprised the control subjects. They were not only spouses of the present patients but also spouses of other patients with advanced AD. These control subjects were known not to have manifested cognitive changes during the follow-up period of >2 y, since these spouses were attendant for the AD patients. We were also cognizant of their mental health. The Ethics Committee of the National Center of Neurology and Psychiatry approved this study, and all subjects gave informed consent to participate.

We randomly divided these subjects into 2 groups. The first group was used to identify the brain area with significant decreases of rCBF in patients compared with that of healthy control subjects. The second group was used then to compare the discrimination ability between patients and control subjects by 3D-SSP with that of visual inspection in regions identified in the first group.

SPECT image data in the present study have previously been reported in 12 of the 38 patients and 25 of the 76 healthy volunteers (*4*).

TABLE 1
Mean Performance Levels in Neuropsychologic Assessment

Subject	Sex F:M	Age (y)	Education (y)	Years after baseline study	MMSE	Digit span		Word learning (10 words), delayed recall (30 min)	Story recall (15 elements)		Ray–Osterrieth complex figure test	
						Forward	Backward		Immediate	Delayed (30 min)	Copy	Recall
												Immediate	Delayed (30 min)
Healthy volunteers	39:37	71.0 ± 7.1	12.0 ± 2.7		27.8 ± 2.4	5.3 ± 0.6	4.2 ± 0.7	8.0 ± 1.0	9.6 ± 3.6	8.0 ± 2.7	35.6 ± 0.8	19.9 ± 4.3	18.8 ± 5.6
Early AD patients	22:16	71.1 ± 8.4	11.9 ± 2.6										
Baseline					26.1 ± 1.6*	5.3 ± 0.9	3.9 ± 0.8*	1.3 ± 2.2†	5.0 ± 2.6†	0.8 ± 1.7†	33.5 ± 5.7*	7.9 ± 4.4†	5.6 ± 4.9†
1st follow-up				1.2 ± 0.3	22.0 ± 3.7†‡	5.2 ± 0.9	3.8 ± 0.9†	1.2 ± 2.4†	4.5 ± 2.1†	0.5 ± 1.4†	31.2 ± 8.0†	6.8 ± 4.8†	4.1 ± 4.9†§
2nd follow-up				2.3 ± 0.6	19.9 ± 5.3†‡	5.3 ± 1.1	3.5 ± 1.2†	0.3 ± 1.1†‡	3.5 ± 2.4†‡	0.2 ± 1.1†§	29.2 ± 10.1†§	15.3 ± 5.2†‡	2.8 ± 4.2†‡

*Scores of AD patients differ from those of healthy volunteers, $P < 0.05$ (Student t test).
†Scores of AD patients differ from those of healthy volunteers, $P < 0.01$ (Student t test).
‡Scores of 1st or 2nd follow-up study differ from baseline study, $P < 0.01$ (repeated measurement ANOVA with Dunnet test as posthoc multiple comparison).
§Scores of 1st or 2nd follow-up study differ from baseline study, $P < 0.05$ (repeated measurement ANOVA with Dunnet test as posthoc multiple comparison).
Data are mean ± SD in healthy volunteers ($n = 76$) or early AD patients ($n = 38$).

SPECT

Before the SPECT scan was performed, all subjects had an intravenous line established. They were injected while lying down in the supine position with eyes closed in a dimly lit, quiet room. Each subject received an intravenous injection of 600 MBq ^{99m}Tc-ethylcysteinate dimer (^{99m}Tc-ECD). Ten minutes after the injection of ^{99m}Tc-ECD, brain SPECT was performed using triple-head rotating γ-cameras (Multispect3; Siemens Medical Systems, Inc.) equipped with high-resolution fanbeam collimators. For each camera, projection data were obtained in a 128 × 128 format for 24 angles at 50 s per angle. A Shepp and Logan Hanning filter was used for SPECT image reconstruction at 0.7 cycle/cm. Attenuation correction was performed using Chang's method.

Determination of Regions with Significant Decline of rCBF in AD

We randomly selected 19 patients and 38 healthy volunteers as the first group to establish regions with significant decline of rCBF in patients using group analysis by 3D-SSP. Each SPECT image was anatomically standardized to match a standard atlas brain (*15*) while preserving regional perfusion quantity. Maximum cortical activity was extracted to adjacent predefined surface pixels on a pixel-by-pixel basis using a 3D-SSP technique (*16*). The extracted cortical perfusion for patients was compared with that of healthy volunteers using a 2-sample Student *t* test on a pixel-by-pixel basis for approximately 16,000 predefined surface pixels covering the entire cortex. Calculated *t* values were converted to *Z* values using a probability integral transformation for comparison. A statistical significance threshold for $P = 0.05$ was calculated on the 3D-SSP *Z* map using a unified formula that controls multiple pixel comparison and a shape of the stochastic process on the 3D-SSP format (*17*).

Automated Analysis Using 3D-SSP

In the second half group, each SPECT image of the patients on both the baseline and the follow-up studies was compared with the mean and SD of SPECT images of the 38 healthy volunteers using voxel-by-voxel *Z*-score analysis after pixel normalization to values of 5 reference regions: global mean, pontine, cerebellar, sensorimotor, and thalamus; *Z* score = ([control mean] − [individual value])/(control SD) as previously reported by Minoshima et al. (*16*).

Each SPECT image of 1 of the 38 healthy volunteers was also compared with the averaged SPECT image of the remaining 37 healthy volunteers in the same manner as in the patients. Using the averaged value of positive *Z* scores in regions with significant decline of rCBF identified in the first group as the threshold, receiver operating characteristic (ROC) curves were determined using the ROCKIT 0.9β program developed by Metz et al. (http://xray.bsd.uchicago.edu/krl) (*18*). The program calculates the area under the ROC curves (Az), accuracy, sensitivity, and specificity. Accuracy was determined as the value at the point where the sensitivity is the same as the specificity on the ROC curve. The program also tests differences in Az between 3D-SSP and visual inspection. The Games–Howell test was used as the multiple comparison method of Az for specific areas and reference regions. Then, using the PlotROC program (http://xray.bsd.uchicago.edu/krl), interpolated values were also statistically calculated for drawing ROC curves.

Analysis with Visual Inspection

The observers comprised 6 medical doctors with experience in nuclear medicine for at least a year: 4 diagnostic radiologists with careers extending to 20, 16, 6, and 3 y, and 2 physicians working in nuclear medicine for 4 y and 1 y. Before the observers worked independently, a 10-min explanation was provided with regions identified in the first group, which were shown to teach where rCBF typically decreases in AD patients in the early stage. After this teaching session, transaxial, coronal, and sagittal sections of the original SPECT images in the second group were randomly presented to the observers. All of the observers were informed that these SPECT images originated from early AD patients and healthy volunteers. Images of healthy volunteers were intermingled with images of patients. The observers scaled the rCBF decrease into 5 levels in all of the specific areas. Five categories (definite decrease, possible decrease, equivocal decrease, possibly no decrease, and definitely no decrease) were used to describe these 5 levels of brain perfusion decrease. Finally, the observers also judged whether the presented SPECT images were those of the AD patients with 5 categories of certainty: definitely, possibly, equivocally, possibly no, and definitely no. To take the intraobserver variance into account, the observers judged the images twice in the same manner at intervals of >2 wk.

For the intra- and interobserver reliability trials, Spearman ρ-scores and 2-way random-effect intraclass correlation coefficients (ICCs) were calculated using SPSS statistical software (SPSS Inc.). These scores and coefficients for all images of AD patients and healthy volunteers were calculated separately in each specific area. ICC values of <0.4 were deemed as representing poor reliability, 0.4–0.75 as fair to good reliability, and >0.75 as excellent reliability.

RESULTS

Determination of Regions with Significant Decline of rCBF in AD

In the first group, the group comparison at the baseline study showed a significant ($P < 0.05$) rCBF reduction in 2 specific areas—namely, the posterior cingulate gyri and precunei and parietal association cortex. The follow-up SPECT study revealed 3 additional specific areas with rCBF reduction: lower and medial temporal areas, temporal association cortex, and anterior cingulate gyri (Fig. 1). Regions of interest (ROIs) were drawn over 5 specific areas (Fig. 2) using OSIRIS (University Hospital of Geneva, Geneva, Switzerland) with the consent of 2 operators: (1) 2 ROIs in bilateral medial views for the posterior cingulate gyri and precunei; (2) 6 ROIs in bilateral lateral, medial, and inferior views for lower and medial temporal areas; (3) 6 ROIs in bilateral lateral, superior, and posterior views for parietal association cortex; (4) 4 ROIs in bilateral lateral and posterior views for temporal association cortex; and (5) 2 ROIs in bilateral medial views for anterior cingulate gyri. ROI sizes ranged from 54 to 543 pixels. These ROIs were confirmed to be at a quite similar location wherever the reference area for pixel normalization was chosen.

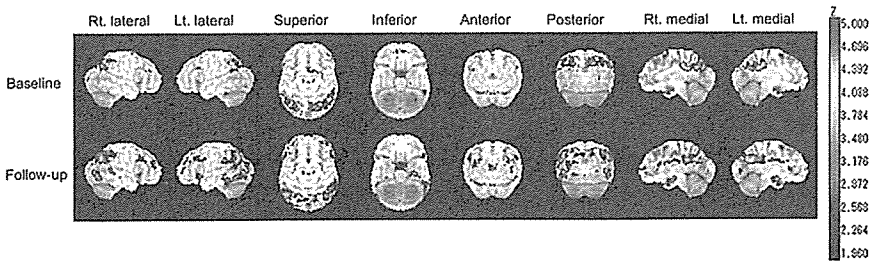

FIGURE 1. Decrease of rCBF adjusted to global mean cerebral blood flow, shown by group analysis of 3D-SSP in patients with early AD at baseline study (top row) and follow-up study (bottom row) compared with healthy volunteers ($P < 0.05$, with multiple comparisons). Rt. = right; Lt. = left.

Comparative Analysis of ROC Curves Between 3D-SSP and Visual Inspection

Table 2 shows Az by 3D-SSP with SEs for 5 specific areas with different reference regions. We averaged positive *Z*-score values across the pixels within each ROI and then chose the highest value among these averaged *Z* scores in ROIs belonging to each specific area. There were no significant differences in Az among the reference regions used for pixel normalization after pooling specific areas at both the baseline and follow-up studies. At the baseline study, although there were no significant differences in Az among the specific areas after pooling reference regions, posterior cingulate gyri and precunei showed greater Az than any other specific area with any reference region. At the follow-up study, posterior cingulate gyri and precunei still showed greater Az than other specific areas except for lower and medial temporal areas. From these results, Az for discrimination of AD patients and control subjects by 3D-SSP was defined as the same value as Az for posterior cingulate gyri and precunei with global mean normalization.

In visual inspection, significant ρ-scores between the first and second trials ($P < 0.01$) indicate good intraobserver reliabilities (Fig. 3). Excellent interobserver reliabilities ranging from 0.762 to 0.890 were observed in every specific area and in discrimination of AD patients and control subjects (Table 3).

The ROC curves for discrimination of AD patients and control subjects were compared between 3D-SSP and visual inspection (Fig. 4). Az values for 3D-SSP in the posterior cingulate gyri were greater than those for visual inspection.

In Figure 5, Az values of the first trial of visual inspection were compared with Az values of 3D-SSP with global mean normalization. At the baseline study, 3D-SSP results in the posterior cingulate gyri and precunei showed significantly higher Az ($P < 0.05$) than results by visual inspection for the discrimination of AD patients and control subjects in all observers. At the follow-up study, all observers showed lower Az values for the discrimination than 3D-SSP. In all specific areas, Az values of all observers were lower than those of 3D-SSP at both the baseline and the follow-up studies.

Table 4 shows the accuracy when sensitivity is equal to specificity. In 3D-SSP, the maximum accuracy of 86.2% was obtained in the posterior cingulate gyri and precunei with reference to the global mean. This accuracy was higher than the maximum accuracy of 74.0% in visual inspection for the discrimination of AD patients and control subjects at the baseline study. At the follow-up study, an accuracy of 74.0% was observed in the posterior cingulate gyri and precunei with reference to the global mean in 3D-SSP, which is still higher than the maximum accuracy of 65.9% in visual inspection.

DISCUSSION

Burdette et al. (*7*) corroborated improvement of diagnostic performance using 3D-SSP in an ^{18}FDG PET study on probable AD patients. In the present study, we confirmed this improvement in AD patients limited to the very early stage using ^{99m}Tc-ECD SPECT, which is more widely performed than PET worldwide. 3D-SSP has been reported to be less affected by the presence of atrophy than SPM (*19*). This method yielded a higher accuracy, even in parietal association cortical areas, than visual inspection, in which metabolic reduction is reported to be the best discriminator of patients with probable AD from healthy volunteers (*16*).

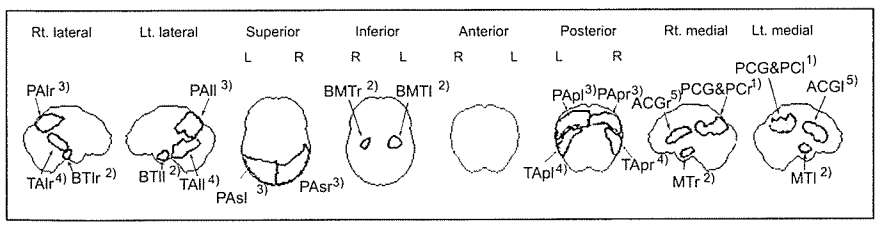

FIGURE 2. ROIs drawn over areas with significant decrease of rCBF in early AD. ROIs were classified into 5 specific areas as follows (numbers with open parentheses denote numbers of pixels included in ROIs): (1) posterior cingulate gyri and precunei: PCG&PC (r = 321 pixels, l = 280 pixels); (2) lower and medial temporal areas: MT (medial temporal areas) (r = 82 pixels, l = 79 pixels), BMT (basal medial temporal area) (r = 60 pixels, l = 112 pixels), and BTI (lateral basal temporal area) (r = 54 pixels, l = 74 pixels); (3) parietal association cortex: PAI (lateral parietal association cortex) (r = 279 pixels, l = 174 pixels), PAp (posterior parietal association cortex) (r = 320 pixels, l = 439 pixels), and Pas (superior parietal association cortex) (r = 543 pixels, l = 496 pixels); (4) temporal association cortex: TAI (lateral temporal association cortex) (r = 172 pixels, l = 367 pixels), TAp (posterior temporal association cortex) (r = 223 pixels, l = 241 pixels); (5) anterior cingulate gyri: ACG (r = 188 pixels, l = 256 pixels).

TABLE 2
Areas Under ROC Curves (Az) for Specific Areas with Different Reference Regions Obtained from 3D-SSP Analysis

Baseline study reference region	Az of specific area				
	PCG&PC	PA	MT	TA	ACG
Global mean	0.937 (0.035)	0.786 (0.080)	0.801 (0.064)	0.766 (0.074)	0.782 (0.065)
Pons	0.814 (0.067)	0.717 (0.076)	0.670 (0.078)	0.605 (0.084)	0.756 (0.066)
Cerebellum	0.897 (0.046)	0.825 (0.063)	0.830 (0.058)	0.768 (0.066)	0.791 (0.066)
Sensorimotor	0.794 (0.059)	0.661 (0.072)	0.605 (0.086)	0.462 (0.087)	0.704 (0.072)
Thalamus	0.819 (0.060)	0.743 (0.070)	0.690 (0.080)	0.662 (0.071)	0.698 (0.082)
Follow-up study reference region	**Az of specific area**				
	PC	PA	MT	TA	ACG
Global mean	0.839 (0.060)	0.807 (0.063)	0.844 (0.057)	0.801 (0.066)	0.781 (0.069)
Pons	0.833 (0.058)	0.760 (0.068)	0.817 (0.063)	0.753 (0.073)	0.823 (0.060)
Cerebellum	0.836 (0.061)	0.797 (0.067)	0.848 (0.051)	0.833 (0.060)	0.817 (0.063)
Sensorimotor	0.846 (0.056)	0.700 (0.069)	0.794 (0.065)	0.717 (0.080)	0.809 (0.061)
Thalamus	0.868 (0.049)	0.748 (0.067)	0.816 (0.058)	0.758 (0.069)	0.799 (0.064)

PCG&PC = posterior cingulate gyri and precunei; PA = parietal association cortex; MT = lower and medial temporal areas; TA = temporal association cortex; ACG = anterior cingulate gyri.

Data are areas under ROC curves (Az) obtained from 3D-SSP. Numbers in parentheses are of Az. No significant results were observed among reference regions after pooling specific areas using Games–Howell test.

The flow or metabolic reduction in the posterior cingulate gyri and precunei has been established to characterize early-to-moderate AD even after correction of partial-volume effects using segmented MR images (*20*). The present study using 3D-SSP demonstrated that rCBF reduction in this specific area is the most reliable finding for diagnosing very early AD, with a high accuracy of 86.2%. 3D-SSP showed a significantly higher performance than the experienced observers at the baseline study. This specific area is known to be important in memory (*21*). A PET study revealed activation of the retrosplenial area of the cingulate cortex during the episodic memory-encoding tasks (*22*). Clinical evidence of the existence of a brain tumor (*23*) or arteriovenous malformation (*24*) in the retrosplenial cingulate cortex supports the importance of this area in memory function.

Most previous pathologic and morphologic studies suggested that structures within the medial temporal structures—amygdala, hippocampal formation, entorhinal cortex, and parahippocampal and fusiform gyri—are the first to be affected in AD with histologic changes, including amy-

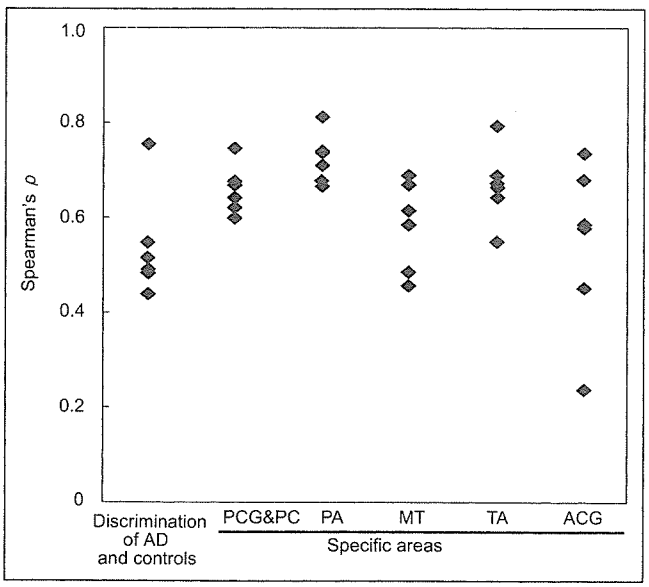

FIGURE 3. Intraobserver reliability between 1st and 2nd trials. ◆, Spearman ρ for individual observer. PCG&PC = posterior cingulate gyri and precunei; PA = parietal association cortex; MT = lower and medial temporal areas; TA = temporal association cortex; ACG = anterior cingulate gyri.

TABLE 3
Interobserver Reliability of Observers

Parameter	Interobserver reliability	
	ICC	95% CI
Discrimination of AD patients and control subjects	0.826	(0.777, 0.867)
Specific area		
PCG&PC	0.805	(0.748, 0.852)
PA	0.890	(0.857, 0.917)
MT	0.819	(0.760, 0.866)
TA	0.864	(0.810, 0.903)
ACG	0.762	(0.649, 0.836)

PCG&PC = posterior cingulate gyri and precunei; PA = parietal association cortex; MT = lower and medial temporal areas; TA = temporal association cortex; ACG = anterior cingulate gyri.

Data in parentheses are 95% confidence intervals (CIs).

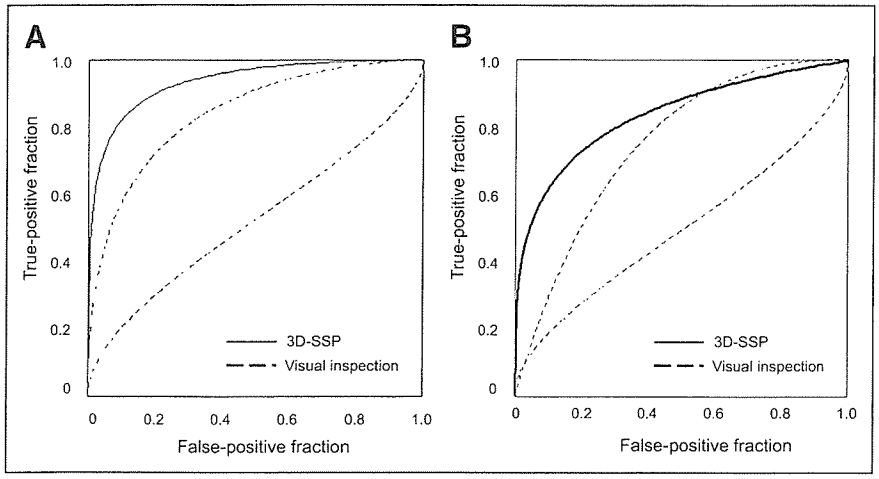

FIGURE 4. ROC curves obtained from 3D-SSP with global mean normalization when thresholding at highest value among averaged positive *Z* scores for ROIs belonging to posterior cingulate gyri and precunei and ROC curves for discrimination of AD patients and control subjects obtained from most excellent and poorest observers for either first or second reading. (A) Baseline study. (B) Follow-up study.

loid deposits and neurofibrillary changes (*5,25–27*). The reduced rCBF in the medial temporal structures demonstrated by PET (*27*) or by a recent high-resolution SPECT system is consistent with these pathologic findings (*28,29*). In the present study, 3D-SSP revealed rCBF reduction in the lower and medial temporal areas more accurately in the follow-up study than in the baseline study. This finding is consistent with our longitudinal results using SPM, in which a significant reduction of hippocampal blood flow did not appear until the mean score of MMSE decreased from 26.2 to 22.3 (*4*). Even in the follow-up study, visual inspection showed significantly lower performance in this specific area than 3D-SSP. This may be because of inherent low accumulation of ^{99m}Tc-ECD in the medial temporal lobes (*30*).

In the present study, rCBF decrease was observed in the anterior cingulate gyri, as well as the posterior cingulate gyri, more prominently in the follow-up study. After involvement of the medial temporal structures, neuropathologic findings such as amyloid deposits and neurofibrillary changes have been observed to spread to the basal forebrain and anterior cingulate gyri, even in the clinically incipient stage of AD, becoming more conspicuous as the disease progresses (*31*). Decreased rCBF in the anterior cingulate gyrus has been reported in subjects with questionable AD at baseline SPECT who converted to AD on follow-up (*3*). Attention must be paid to the possibility of pseudo rCBF reduction produced in structures near the dilated ventricles by mismatches at the edges of the ventricles (*19*). However, for the clinical purpose of diagnosing AD, partial-volume effects may increase the sensitivity of detection of rCBF reduction. Current evidence suggests that after an initial amnesic stage in AD, attention is the first nonmemory domain to be affected before deficits in language and visuospatial function (*32*). In AD it appears that divided attention is particularly vulnerable, while sustained attention is relatively well preserved in the early stages (*32,33*). It has been reported that divided attention activates the anterior cingulate gyri, though sustained attention does not (*34,35*).

Concerning the reference regions for pixel normalization in 3D-SSP, Minoshima et al. reported that the pons is a

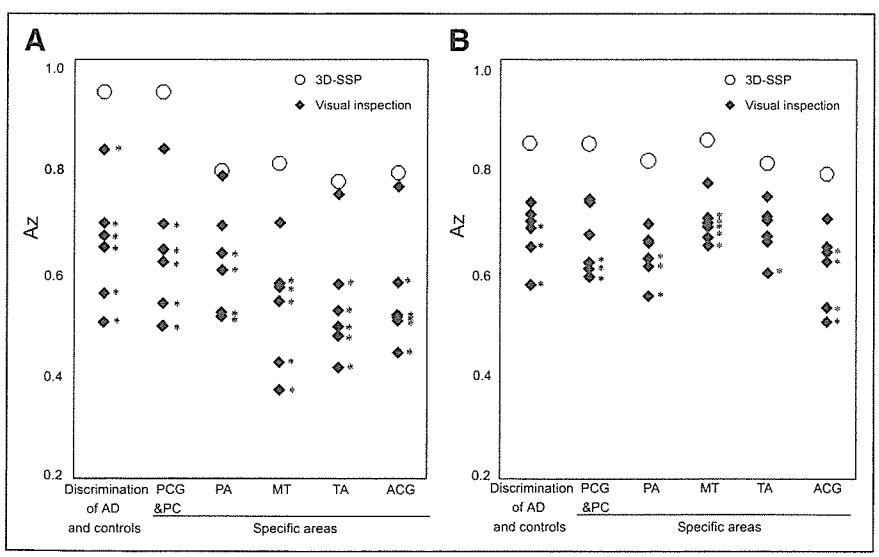

FIGURE 5. Comparison of Az between observers' first visual inspection and 3D-SSP with global mean normalization. ◆, Az for individual observer; ○, Az for 3D-SSP. (A) Baseline study. (B) Follow-up study. PCG&PC = posterior cingulate gyri and precunei; PA = parietal association cortex; MT = lower and medial temporal areas; TA = temporal association cortex; ACG = anterior cingulate gyri. *Az of visual inspection is lower than Az by 3D-SSP analysis ($P < 0.05$). Statistical significance between Az values was calculated using ROCKIT program (*18*).

TABLE 4
Accuracies of Observers' Visual Inspection and 3D-SSP Analysis

Baseline study	Accuracies of discrimination of AD patients and control subjects	Accuracies of specific areas				
		PCG&PC	PA	MT	TA	ACG
Visual inspection	0.493–0.740	0.495–0.735	0.487–0.687	0.387–0.618	0.417–0.660	0.437–0.672
3D-SSP reference region						
Global mean	0.862	0.862	0.718	0.712	0.679	0.689
Pons		0.722	0.639	0.602	0.556	0.668
Cerebellum		0.795	0.729	0.730	0.678	0.698
Sensorimotor		0.702	0.599	0.556	0.453	0.573
Thalamus		0.720	0.658	0.618	0.600	0.628
Follow-up study	**Accuracies of discrimination of AD patients and control subjects**	**Accuracies of specific areas**				
		PCG&PC	PA	MT	TA	ACG
Visual inspection	0.530–0.659	0.541–0.654	0.538–0.616	0.585–0.676	0.547–0.661	0.479–0.622
3D-SSP reference region						
Global mean	0.740	0.740	0.710	0.744	0.706	0.690
Pons		0.733	0.671	0.72	0.667	0.742
Cerebellum		0.738	0.703	0.766	0.734	0.720
Sensorimotor		0.745	0.631	0.7	0.641	0.711
Thalamus		0.765	0.662	0.719	0.669	0.704

PCG&PC = posterior cingulate gyri and precunei; PA = parietal association cortex; MT = lower and medial temporal areas; TA = temporal association cortex; ACG = anterior cingulate gyri.

Data are accuracies when sensitivity is equal to specificity in ROC analysis. Accuracies of visual inspection are described as a range from minimum to maximum at the first trial.

reliable reference for data normalization on quantitative ^{18}F-FDG PET measurement (*36*). In our study, Az did not show significant differences among reference regions. In the case of SPECT, the pons may be at the margin of spatial resolution for adequate and stable counts. Although rCBF in the cerebellum has been reported to decrease in advanced AD patients (*37*), the choice of cerebellum for pixel normalization would be acceptable in mild or very early AD. Subsequently, Minoshima et al. used the thalamus as a reference region (*16*) based on their prior observation that the thalamus or primary sensorimotor cortex is more suitable than the global mean or cerebellum. They also reported that the thalamus has a distinct shape and is located just above the intercommissural line, the standard line defining the stereotactic coordinate system, thereby ensuring reliable and accurate localization. Bartenstein et al. (*38*) used thalamic normalization even though they showed that global normalization resulted in the least mean cortical coefficients of variation in ^{99m}Tc-ECD SPECT. They considered global normalization to be inappropriate for a disease such as AD with widespread metabolic or flow reduction and concluded that the thalamus is the most robust reference region for SPECT images. However, the thalamus is pathologically known to be involved from an early stage (*25*). Moreover, Johnson et al. (*3*) revealed a rCBF decrease in the anterior thalamus in subjects with questionable AD at baseline SPECT who converted to AD on follow-up. We considered that global normalization is sufficient for routine clinical discrimination of early AD patients and control subjects. The present results confirmed the highest accuracy using global normalization at the baseline study.

Finally, we must refer to limitations of this kind of study even when conducted in the best situation (a specialized clinic for memory disorders). It has been reported that the clinical diagnosis of probable AD is 80%–90% accurate when compared with final pathologic verification (*39*), although prolonged follow-up with serial evaluation was performed to diagnose AD clinically in the present study.

CONCLUSION

A 3D-SSP technique using a normal database of brain perfusion SPECT images can detect a slight rCBF decrease in the posterior cingulate gyri and precunei with higher ability to discriminate very early AD patients from healthy control subjects than visual inspection. This technique afforded the maximum discrimination of 86.2% in accuracy at the very early stage corresponding to MCI. On the other hand, the maximum accuracy of visual interpretation was >10% lower as compared with 3D-SSP. The present results suggest that it is clinically useful and reliable to adopt the use of artificial computer intelligence as an adjunct to visual image interpretation for dementia evaluation.

ACKNOWLEDGMENTS

This study was supported by Comprehensive Research on Aging and Health, grant H13-choju-004 from the Ministry of Health, Labor and Welfare. The authors are very thankful to Prof. Satoshi Minoshima (University of Washington) and Dr. Toru Matsumoto (National Institute of Radiologic Sciences) for valuable suggestions regarding the theory of 3D-SSP and ROC curve analysis, respectively; Dr. Toru Kinoshita (Department of Biostatistics, School of Health Sciences and Nursing, University of Tokyo) for statistics; John Gelblum for proofreading this manuscript; and the technical staff in our hospital for data acquisition.

REFERENCES

1. Minoshima S, Foster NL, Kuhl DE. Posterior cingulate cortex in Alzheimer's disease. *Lancet.* 1994;344:895.
2. Minoshima S, Giordani B, Berent S, et al. Metabolic reduction in the posterior cingulate cortex in very early Alzheimer's disease. *Ann Neurol.* 1997;42:85–94.
3. Johnson KA, Jones BL, Holman JA, et al. Preclinical prediction of Alzheimer's disease using SPECT. *Neurology.* 1998;50:1563–1571.
4. Kogure D, Matsuda H, Ohnishi T, et al. Longitudinal evaluation of early Alzheimer's disease using brain perfusion SPECT. *J Nucl Med.* 2000;41:1155–1162.
5. Brun A, Gustafson L. Distribution of cerebral degeneration in Alzheimer's disease: a clinico-pathological study. *Arch Psychiatr Nervenkr.* 1976;223:15–33.
6. Gerard E, Konrad B, Colin LM, Jean-Marie M. Prospects for pharmacological intervention in Alzheimer disease. *Arch Neurol.* 2000;57:454–459.
7. Burdette JH, Minoshima S, Borght TV, Tran DD, Kuhl DE. Alzheimer disease: improved visual interpretation of PET images by three-dimensional stereotaxic surface projections. *Radiology.* 1996;198:837–843.
8. Frackowiak RSJ, Friston KJ, Frith CD, Dolan RJ, Mazziotta JC. *Human Brain Function.* 1st ed. San Diego, CA: Academic Press; 1997.
9. Ishii K, Sasaki M, Yamaji S, Sakamoto S, Kitagaki H, Mori E. Demonstration of decreased posterior cingulate gyrus correlates with disorientation for time and place in Alzheimer's disease by means of $H_2{}^{15}O$ positron emission tomography. *Eur J Nucl Med.* 1997;24:670–673.
10. McKhann G, Drachman D, Folstein M, Katzman R, Prie D, Stadlan EM. Clinical diagnosis of Alzheimer's disease: report of the NINCDS-ADRDA Work Group under the auspices of Department of Health and Human Services Task Force on Alzheimer's Disease. *Neurology.* 1984;34:939–944.
11. Hodges JR. *Cognitive Assessment for Clinicians.* 1st ed. Oxford, U.K.: Oxford Medical Publication; 1993.
12. Petersen RC, Dooby R, Kurz A, et al. Current concepts in mild cognitive impairment. *Arch Neurol.* 2001;58:1985–1992.
13. Hughes CP, Berg L, Danziger WL, Coben LA, Martin RL. A new clinical scale for the staging of dementia. *Br J Psychiatry.* 1982;140:566–572.
14. Folstein MF, Folstein SE, McHugh PR. Mini-Mental State: a practical method for grading the cognitive state of patients for the clinician. *J Psychiatr Res.* 1975; 12:189–198.
15. Minoshima S, Koeppe RA, Frey KA, Kuhl DE. Anatomic standardization: linear scaling and nonlinear warping of functional brain images. *J Nucl Med.* 1994;3: 1528–1537.
16. Minoshima S, Frey KA, Koeppe RA, et al. A diagnostic approach in Alzheimer's disease using three-dimensional stereotactic surface projections of fluorine-18-FDG PET. *J Nucl Med.* 1995;36:1238–1248.
17. Worsley KJ, Marrett S, Neelin P, et al. A unified statistical approach for determining significant signals in location and scale space images of cerebral activation. In: Myers R, Cunningham V, Baily D, et al, eds. *Quantification of Brain Function Using PET.* San Diego, CA: Academic Press; 1996:327–333.
18. Metz CE, Herman BA, Roe CA. Statistical comparison of two ROC-curve estimates obtained from partially-paired datasets. *Med Decis Making.* 1998;18: 110–121.
19. Ishii K, Willoch F, Minoshima S, et al. Statistical brain mapping of ^{18}F-FDG PET in Alzheimer's disease: validation of anatomic standardization for atrophied brains. *J Nucl Med.* 2001;42:548–557.
20. Ibanez V, Pietrini P, Alexandar GE, et al. Regional glucose metabolic abnormalities are not the result of atrophy in Alzheimer's disease. *Neurology.* 1998;50: 1585–1593.
21. Desgranges B, Baron JC, de la Sayette V, et al. The neural substrates of memory systems impairment in Alzheimer's disease: a PET study of resting brain glucose utilization. *Brain.* 1998;121:611–631.
22. Fletcher PC, Frith CD, Grasby PM, Shallice T, Frackwiak RSJ, Dolan RJ. Brain system for encoding and retrieval of auditory-verbal memory. *Brain.* 1995;118: 401–416.
23. Rudge P, Warrington EK. Selective impairment of memory and visual perception in splenial tumours. *Brain.* 1991;114:349–360.
24. Valenstein E, Bowers D, Verfaellie M, Heilman KM, Day A, Watson RT. Retrosplenial amnesia. *Brain.* 1987;110:1631–1646.
25. Braak H, Braak E. Neuropathological staging of Alzheimer-related changes. *Acta Neuropathologica.* 1991;82:239–256.
26. Gomez-Isla T, Price TL, McKeel DW, Morris JC, Growdon JH, Hyman BT. Profound loss of layer II entorhinal cortex neurons occurs in very mild Alzheimer's disease. *J Neurosci.* 1996;16:4491–4500.
27. Pearlson GD, Harris GJ, Powers RE, et al. Quantitative changes in mesial temporal volume, regional cerebral blood flow, and cognition in Alzheimer's disease. *Arch Gen Psychiatry.* 1992;49:402–408.
28. Ohnishi T, Hoshi H, Nagamachi S, et al. High-resolution SPECT to assess hippocampal perfusion in neuropsychiatric diseases. *J Nucl Med.* 1995;36:1163–1169.
29. Julin P, Lindqvist J, Svensson L, Slomka P, Wahlund LO. MRI-guided SPECT measurements of medial temporal lobe blood flow in Alzheimer's disease. *J Nucl Med.* 1997;38:914–919.
30. Oku N, Matsumoto M, Hashikawa K, et al. Intra-individual differences between technetium-99m-HMPAO and technetium-99m-ECD in the normal medial temporal lobe. *J Nucl Med.* 1997;38:1109–1111.
31. Jack CR, Petersen RC, Xu YC, et al. Medial temporal atrophy on MRI in normal aging and very mild Alzheimer's disease. *Neurology.* 1997;49:786–794.
32. Perry RJ, Hodges JR. Attention and executive deficits in Alzheimer's disease: a critical review. *Brain.* 1999;122:383–404.
33. Rizzo M, Anderson SW, Dawson J, Myers R, Ball K. Visual attention impairments in Alzheimer's disease. *Neurology.* 2000;54:1954–1959.
34. Corbetta M, Miezin FM, Dobmeyer S, Shulman GL, Pertersen SE. Selective and divided attention during visual discrimination of shape, color, and speed: functional anatomy by positron emission tomography. *J Neurosci.* 1991;11:2383–2402.
35. Iidaka T, Anderson ND, Kapur S, Cabeza R, Craok FI. The effect of divided attention on encoding and retrieval in episodic memory revealed by positron emission tomography. *J Cogn Neurosci.* 2000;12:267–280.
36. Minoshima S, Frey KA, Foster NL, Kuhl DE. Preserved pontine glucose metabolism in Alzheimer disease: a reference region for functional brain image (PET) analysis. *J Comput Assist Tomogr.* 1995;19:541–547.
37. Ishii K, Sasaki M, Kitagaki H, et al. Reduction of cerebellar glucose metabolism in advanced Alzheimer's disease. *J Nucl Med.* 1997;38:925–928.
38. Bartenstein P, Minoshima S, Hirsch C, et al. Quantitative assessment of cerebral blood flow in patients with Alzheimer's disease by SPECT. *J Nucl Med.* 1997; 38:1095–1101.
39. Adams RD. Alzheimer's disease. In: Adams RD, Victor M, Ropper AH, eds. *Principles of Neurology.* 6th ed. New York, NY: McGraw-Hill; 1997:1049–1057.

Effects of partial volume correction on discrimination between very early Alzheimer's dementia and controls using brain perfusion SPECT

Hidekazu Kanetaka[1, 4], Hiroshi Matsuda[1], Takashi Asada[2], Takashi Ohnishi[1], Fumio Yamashita[2], Etsuko Imabayashi[1], Fumiko Tanaka[1], Seigo Nakano[3], Masaru Takasaki[4]

[1] Department of Radiology, National Center Hospital for Mental, Nervous and Muscular Disorders, National Center of Neurology and Psychiatry, Kodaira, Tokyo, Japan
[2] Department of Neuropsychiatry, Institute of Clinical Medicine, University of Tsukuba, Tsukuba, Ibaraki, Japan
[3] Department of Geriatric Medicine, National Center Hospital for Mental, Nervous and Muscular Disorders, National Center of Neurology and Psychiatry, Kodaira, Tokyo, Japan
[4] Department of Geriatric Medicine, Tokyo Medical University, Shinjuku, Tokyo, Japan

Received: 25 December 2003 / Accepted: 9 February 2004 / Published online: 28 February 2004

Abstract. We assessed the accuracy of brain perfusion single-photon emission computed tomography (SPECT) in discriminating between patients with probable Alzheimer's disease (AD) at the very early stage and age-matched controls before and after partial volume correction (PVC). Three-dimensional MRI was used for PVC. We randomly divided the subjects into two groups. The first group, comprising 30 patients and 30 healthy volunteers, was used to identify the brain area with the most significant decrease in regional cerebral blood flow (rCBF) in patients compared with normal controls based on the voxel-based analysis of a group comparison. The second group, comprising 31 patients and 31 healthy volunteers, was used to study the improvement in diagnostic accuracy provided by PVC. A Z score map for a SPECT image of a subject was obtained by comparison with mean and standard deviation SPECT images of the healthy volunteers for each voxel after anatomical standardization and voxel normalization to global mean or cerebellar values using the following equation: Z score = ([control mean]–[individual value])/(control SD). Analysis of receiver operating characteristics curves for a Z score discriminating AD and controls in the posterior cingulate gyrus, where a significant decrease in rCBF was identified in the first group, showed that the PVC significantly enhanced the accuracy of the SPECT diagnosis of very early AD from 73.9% to 83.7% with global mean normalization. The PVC mildly enhanced the accuracy from 73.1% to 76.3% with cerebellar normalization. This result suggests that early diagnosis of AD requires PVC in a SPECT study.

Keywords: SPECT – Alzheimer's disease – Regional cerebral blood flow – ^{99m}Tc-ECD – Partial volume correction

Eur J Nucl Med Mol Imaging (2004) 31:975–980
DOI 10.1007/s00259-004-1491-3

Hiroshi Matsuda (✉)
Department of Radiology,
National Center Hospital for Mental,
Nervous and Muscular Disorders,
National Center of Neurology and Psychiatry,
4-1-1 Ogawahigashi, 187-8551 Kodaira, Tokyo, Japan
e-mail: matsudah@ncnpmusashi.gr.jp
Tel.: +81-42-3412711, Fax: +81-42-3461736

Introduction

The fact that recently available medications such as cholinesterase inhibitors delay the progression of Alzheimer's disease (AD) has increased the urgency of diagnosing AD at an earlier stage. Although recent advances in the computer-assisted statistical analysis of positron emission tomography (PET) or single-photon emission computed tomography (SPECT) after anatomical image standardization have made it easier to detect regional metabolic or perfusion changes in the early stage of AD [1, 2, 3, 4], there have been few studies on the diagnostic performance of SPECT in very early AD.

The more limited spatial resolution of SPECT scanners as compared with that of PET does not allow an exact measurement of the local radiotracer concentration in brain tissue since partial volume effects cause underestimation of activity in small structures of the brain. Since brain atrophy accentuates the partial volume effects on SPECT measurements, actual regional cerebral blood